PERGAMON

Journal of Structural Geology 22 (2000) 1009–1014

JOURNAL OF STRUCTURAL GEOLOGY

www.elsevier.nl/locate/jstrugeo

Velocity field for the trishear model

Alan T. Zehnder[a,*], Richard W. Allmendinger[b]

[a]*Department of Theoretical and Applied Mechanics, Cornell University, Ithaca, NY 14853, USA*
[b]*Department of Geological Sciences, Cornell University, Ithaca, NY 14853, USA*

Received 19 October 1999; accepted 8 March 2000

Abstract

A general method for the derivation of velocity fields consistent with the basic kinematics of the trishear model of fault-propagation folding is given. We show that the fields can be written as explicit functions of position within the deformation zone. To demonstrate the approach, several different linear and non-linear velocity fields are derived and plotted. We show that the trishear zone need not be symmetric and that the trishear model produces $1/r$ singular strain rates, consistent with results for cracks in elastic–plastic materials. A continuous formulation of heterogeneous trishear is also presented.

1. Introduction

The trishear model (Erslev, 1991) provides an important alternative to the better known parallel kink model (Suppe and Medwedeff, 1990) of fault-propagation folding. Erslev and coworkers (Erslev, 1991; Erslev and Rogers, 1993; Erslev and Mayborn, 1997) have shown that numerous well-documented structures of the Rocky Mountain foreland and elsewhere qualitatively resemble simple numerical forward models of trishear geometry. Allmendinger (1998) presented a numerical inverse grid search, providing a quantitative, scientifically objective way of applying trishear to real structures.

Trishear has been previously presented in both geometric (Erslev, 1991; Erslev and Rogers, 1993) and approximate velocity-based (Hardy and Ford, 1997) formulations. In addition, Erslev (1991) briefly describes a method for producing 'heterogeneous' trishear in which strain is more concentrated towards the center of the trishear zone. All previous papers on trishear have suggested that the trishear zone must be symmetric with respect to the fault in order to maintain area balance. Hardy and Ford (1997), Allmendinger (1998) and Hardy and McClay (1999) explored the influence of (P/S), the ratio of fault tip propagation speed to slip rate.

Here we present a precise, simple, and generalizable method for deriving velocity fields for the trishear model. The method is based on requiring that the velocity field be divergence free (to conserve area). We show that an infinite number of potential fields can be found which satisfy the boundary conditions of the basic trishear model. This permits the derivation of asymmetric and center-concentrated trishear zones among a myriad of other possibilities. Although a mechanical analysis remains to be done, some of our results are consistent with those from analyses of cracks in elastic–perfectly plastic material. Eventually, the approach will enable one to compare the velocity fields predicted by mechanical models of trishear-like deformation to the kinematic model.

2. Velocity fields

The basic geometry of the trishear model is shown in Fig. 1. A triangular zone of shearing with angles φ_1 and φ_2, both $<90^\circ$, lies between two rigid zones. The

* Corresponding author. Fax: +1-607-255-2011.
E-mail address: atz2@cornell.edu (A.T. Zehnder).

0191-8141/00/$ - see front matter
PII: S0191-8141(00)00037-7

footwall is considered stationary, and the hanging wall moves to the right with speed v_0. The fault tip may move or be stationary. The ratio of the fault propagation speed to slip speed, labeled as (P/S) in Hardy and Ford (1997) and Allmendinger (1998), is an important parameter in determining the final deformation field. The velocity field will be written in vector form as

$$\underline{v}(x, y) = v_x(x, y)\hat{i} + v_y(x, y)\hat{j} \tag{1}$$

where the x and y axes are parallel and perpendicular to the fault line, and $\hat{i}$, $\hat{j}$ are the usual unit vectors in the x and y directions, respectively. The origin of the co-ordinates is attached to the fault tip.

In the hanging wall sector, $\underline{v} = v_0\hat{i}$, in the footwall sector $\underline{v} = \underline{0}$. We now seek to construct a velocity field in the trishear zone that conserves area, is continuous and matches the hanging wall and footwall sector velocities on the top and bottom boundaries of the zone. The boundary conditions are

$$\begin{aligned} &v_x = v_0, \quad v_y = 0, \quad \text{on} \quad y = x\tan\varphi_1, \\ &v_x = 0, \quad v_y = 0, \quad \text{on} \quad y = -x\tan\varphi_2 \end{aligned} \tag{2}$$

The condition that area is conserved, or that the flow is incompressible, is that the divergence of the velocity field is zero, (see for example, Mase and Mase, 1992, p. 132)

$$\text{div}\ \underline{v} \equiv \frac{\partial v_x}{\partial x} + \frac{\partial v_y}{\partial y} = 0. \tag{3}$$

The approach will be to choose a v_x field consistent with Eq. (2), then determine the v_y field from Eqs. (2) and (3). Other than satisfying the boundary conditions and continuity, any reasonable v_x field and any combination of trishear angles can be chosen. Note that Eq. (3) can be stated in three dimensions for analysing three-dimensional deformation.

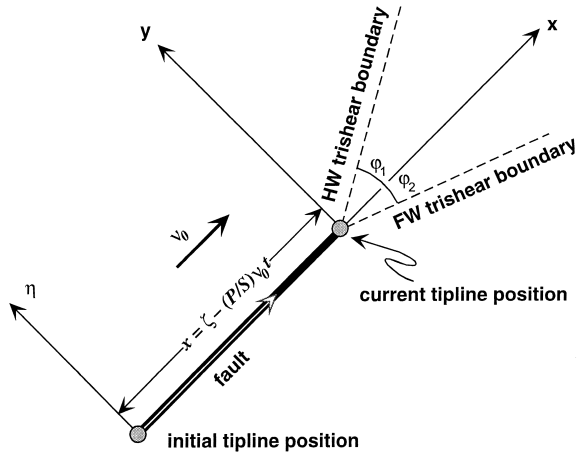

Fig. 1. Geometry of the trishear model showing co-ordinate systems used in the text. Note that the apical angle of the hanging wall and footwall trishear boundaries need not be the same. See text for definition of symbols.

2.1. Symmetric trishear zones

Consistent with the fields used by previous authors, let us start with fields for symmetric trishear zones, $\varphi_1 = \varphi_2 \equiv \varphi$. To simplify writing the equations, let $m = \tan\varphi$. One choice for v_x is

$$\begin{aligned} v_x = \frac{v_0}{2}\left[\text{sgn}\,(y)\left(\frac{|y|}{xm}\right)^{\frac{1}{s}} + 1\right], \quad x > 0, \\ -xm \le y \le xm, \quad s \ge 1, \end{aligned} \tag{4}$$

where sgn (y) denotes the sign of y, and s is a parameter that changes the shape of the field. For $s = 1$ the v_x velocity distribution is linear in y, producing a strain rate that is nearly uniform with respect to y. This field can be derived from the geometric description of 'homogeneous' trishear by Erslev (1991) and is very similar to the Hardy and Ford (1997) field, which is nearly linear in y. As s increases, the deformation concentrates towards the center of the trishear zone, producing non-uniform strain rates, which appears to be analogous to Erslev's 'heterogeneous' trishear. It can easily be seen that the above field satisfies the v_x boundary conditions in Eq. (2). To find v_y, we differentiate Eq. (4) with respect to x, invoke incompressibility, Eq. (3),

$$\frac{\partial v_y}{\partial y} = -\frac{\partial v_x}{\partial x}$$

and integrate with respect to y yielding

$$v_y = \frac{v_0 m}{2(1+s)}\left(\frac{|y|}{mx}\right)^{\frac{(1+s)}{s}} + C. \tag{5}$$

The constant of integration, C, is found by using the boundary conditions given in Eq. (2). The resulting velocity field in the trishear zone is

$$\begin{aligned} \underline{v}(x, y) = \frac{v_0}{2}\Bigg\{&\left[\text{sgn}\,(y)\left(\frac{|y|}{mx}\right)^{\frac{1}{s}} + 1\right]\hat{i} \\ &+ \frac{m}{1+s}\left[\left(\frac{|y|}{mx}\right)^{\frac{(1+s)}{s}} - 1\right]\hat{j}\Bigg\}. \end{aligned} \tag{6}$$

When $s = 1$, the field will be called the 'linear field' (v_x linear in y). Velocity vectors for this case are plotted in Fig. 2(a) for $\varphi = 30°$; for comparison, we also show the velocity field obtained for a non-linear field, $s = 3$, in Fig. 2(b). Note that as $y \to -x\tan\varphi$, $v_y/v_x \to -\tan\varphi$, i.e. as the boundary

between the trishear zone and the footwall is approached, the velocity vectors are parallel to the boundary.

The advantage of the above construction is that now an explicit equation for the velocity field as a function of position (x,y) with respect to the fault tip is given. The resulting deformation field is easily calculated from here by numerical integration. The strain rates can be explicitly calculated. For example, for $s = 1$, the shear strain rate is

$$\dot{\gamma}_{xy} = \frac{1}{2}\left(\frac{\partial v_x}{\partial y} + \frac{\partial v_y}{\partial x}\right) = \frac{v_0}{4xm}\left(1 - \frac{y^2}{x^2}\right). \quad (7)$$

Note that the shear strain rate is singular as $1/x$, i.e. the shear strain rate is infinite as the fault tip is approached. The $1/x$ singularity of strain rate is consistent with the strain singularity of a stationary crack in an elastic–perfectly plastic material (Rice, 1968). It results geometrically from focusing of the trishear boundaries to the fault tip and occurs for any trishear velocity field. When $\varphi > 45^\circ$ there can be regions within the trishear zone where $y > x$, and hence by Eq. (7), $\dot{\gamma}_{xy} < 0$. This does not however produce any strange looking results once the velocity is integrated to simulate the deformation.

Note that one can start with other assumptions for v_x and, invoking incompressibility, derive other velocity fields. For example, if instead of allowing an abrupt change in v_x at the top boundary, we assume a field where v_x changes smoothly as sin y, the following field can be derived

$$\underline{v}(x, y) = v_0\left[\frac{1}{2}(\sin\beta + 1)\hat{i} + \tan\varphi(\cos\beta + \beta\sin\beta - \pi/2)\hat{j}\right], \quad (8)$$

where $\beta = \beta(x, y) \equiv \frac{y\pi}{2x\tan\varphi}$. This will be called the 'sine field' (v_x varies as sin y). The above is but one of an infinity of fields compatible with conservation of area, Eq. (3), and with the boundary conditions, Eq. (2), that could be derived.

2.2. Asymmetric trishear zones

If the v_x field is linear with respect to y, it can be shown that the trishear zone must be symmetric. However, if we allow the v_x field to be piecewise linear, i.e. to consist of one or more connected, linear segments, that can have different slopes, we can relax the restriction to symmetric fields. For example, consider a field with two segments. To simplify writing the equations let $m_1 = \tan\varphi_1$, $m_2 = \tan\varphi_2$. We seek to construct a piecewise linear v_x field with one kink, along $y = 0$, such that $v_x = v_0$ on $y = m_1 x$, $v_x = \lambda v_0$ on $y = 0$, and $v_x = 0$ on $y = -m_2 x$. Such a field can be written in two pieces, both linear with respect to y, as

$$v_x = v_0(1-\lambda)\left[\frac{y}{m_1 x} + \frac{\lambda}{1-\lambda}\right], \quad y > 0$$
$$v_x = v_0\lambda\left[\frac{y}{m_2 x} + 1\right], \quad y < 0. \quad (9a)$$

Using incompressibility, Eq. (3) and matching the boundary conditions, Eq. (2),

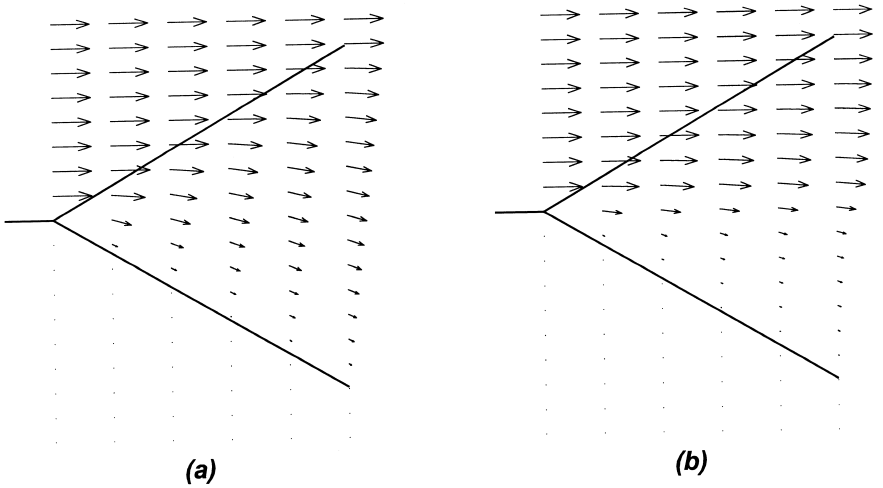

Fig. 2. (a) Velocity vectors for the symmetric, linear v_x field. (b) Velocity vectors for symmetric, non-linear v_x field with $s = 3$.

$$v_y = \frac{v_0(1-\lambda)m_1}{2}\left[\left(\frac{y}{m_1 x}\right)^2 - 1\right], \quad y > 0$$

$$v_y = \frac{v_0\lambda m_2}{2}\left[\left(\frac{y}{m_2 x}\right)^2 - 1\right], \quad y < 0. \tag{9b}$$

The fields must be continuous. Matching the v_y fields at $y = 0$ requires that

$$\lambda = \frac{m_1}{m_1 + m_2}. \tag{9c}$$

When the field is symmetric ($m_1 = m_2$), $\lambda = 1/2$, recovering the linear v_x field. In the limit as $m_2 \to 0$, $\lambda \to 1$, meaning that the zone $y > 0$ slides rigidly while the zone $y < 0$ remains stationary. Note that Eq. (9c) implies that the relative strain rates in the upper and lower zones cannot be chosen independently, they depend on the ratio of m_1 to m_2. Note also that on $y = 0$, $v_y \neq 0$, i.e. there is a flux of material across the boundary between the upper and lower zones. Thus asymmetric trishear does *not* simply represent two trishear zones side-by-side.

3. Simulation of deformation

Given the velocity field, the resulting deformation is easily computed by numerical integration. We introduce two coordinate systems. The (x,y) system is attached to the fault tip and convects to the right at speed $(P/S)v_0$. The (ζ,η) system is stationary. The two systems start with a common origin and are related at time t by $x = \zeta - (P/S)v_0 t$, $y = \eta$, where $(P/S)v_0 t$ is the distance the fault tip has propagated. Note that the velocity field, $\underline{v} = \underline{v}(x,y)$, is given with respect to the moving coordinate system (x,y). Thus when velocity is computed, its arguments in terms of the stationary coordinate system are $(x = \zeta - (P/S)v_0 t,\ y = \eta)$.

Let $\underline{\zeta} \equiv (\zeta,\eta)$ be the current coordinates of a particle. Using simple numerical integration the coordinates at time step $n + 1$ are related to the coordinates at the previous time step, n, by

$$\underline{\zeta}_{n+1} = \underline{\zeta}_n + \underline{v}\left(\zeta_n - \left(\frac{P}{S}\right)v_0 t, \eta_n\right)\Delta t, \tag{10}$$

with $t = n\Delta t$

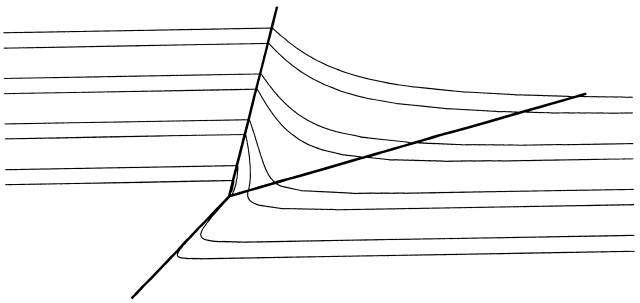

Fig. 3. Deformation resulting from linear field, $s = 1$. Thin lines are bedding tops and thick lines are the fault and the trishear zone boundaries. In all of the plots, Figs. 3–6, $(P/S) = 1$, ramp angle = 45°. Trishear angle, $2\varphi = 60°$ for Figs. 3–5.

3.1. Symmetric trishear deformation

To visualize the deformation produced by the trishear model, a set of points, defining eight bed tops was created, then mapped using Eq. (10). In Figs. 3–5 that follow, $\varphi = 30°$, ramp angle = 45° (the angle between the fault and the initial bed orientation) and $(P/S) = 1$.

To prove that the current results are consistent with previous works, the deformation using the linear velocity field, $s = 1$ in Eq. (6), is plotted in Fig. 3. The resulting picture of fault propagation folding is similar to results shown in Allmendinger (1998) (generated using the method of Hardy and Ford, 1997) and to results shown in Erslev (1991). By varying (P/S), φ and the ramp angle, all of the homogeneous deformation cases demonstrated in Erslev (1991) and Allmendinger (1998) can be reproduced.

As the parameter s is increased, deformation concen-

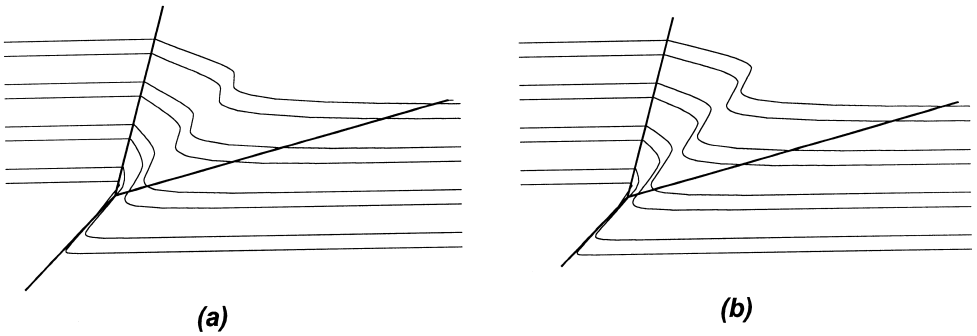

Fig. 4. Deformation resulting from non-linear field, (a) $s = 2$, (b) $s = 3$. As s increases, deformation concentrates towards center of the trishear zone.

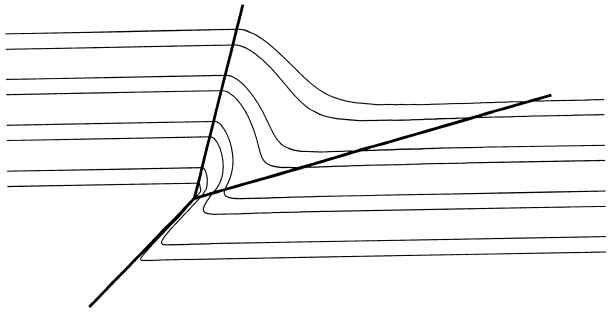

Fig. 5. Deformation resulting from sine field. Note that, even though $P/S = 1$, no sharp kink occurs at the hanging wall boundary of the trishear zone even though this boundary is fixed in the material.

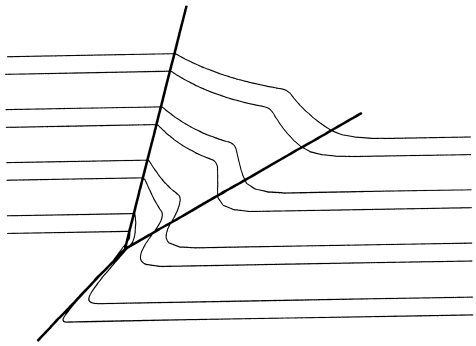

Fig. 6. Deformation resulting from asymmetric linear field using $\tan \varphi_2 = 1/2 \tan \varphi_1, \varphi_1 = 30^\circ$, and placing one kink along $y = 0$.

trates towards the center of the trishear zone. This is shown in Fig. 4 for $s = 2$ and $s = 3$. For $s > 3$, essentially all of the slip is concentrated along a narrow, ductile shear zone in the center of the trishear zone. Erslev (1991) was not explicit about how his examples of 'heterogeneous' trishear were produced, thus we cannot compare our method to his.

Fig. 5 shows that the sine field, Eq. (8), produces results similar to the linear field, but rounds the corners where material enters the trishear zone. This suggests that any v_x more or less similar to the linear field, Eq. (6), is a reasonably good choice in the trishear model.

3.2. Asymmetric trishear deformation

Deformation for an asymmetric trishear zone, Eqs. (9a), (9b) and (9c), is shown in Fig. 6. In this simulation $\varphi_1 = 30^\circ$ and $\tan \varphi_2 = 1/2 \tan \varphi_1$. The resulting deformation has a kink along $y = 0$. Asymmetric trishear has not been demonstrated by any previous worker. Note that non-linear versions of the asymmetric trishear model could be constructed, the location of the kink in v_x could be varied, or there could be any number of kinks in v_x. However, within these variations, the fields are constrained by the matching conditions and by div $\underline{v} = 0$. In the example given, there are no free parameters in the velocity field once m_1 and m_2 are chosen. However, for more than one kink, there are (number of kinks−1) free parameters in the velocity field once the kink locations are chosen. Thus, any velocity field, symmetric or asymmetric, can be constructed using enough linear velocity sectors. In the limit as an infinite number of sectors are taken, a continuous field is obtained, examples of which are given in Eqs. (6) and (8). It may be that piecewise linear fields could simulate some of the kink fault-propagation folds described in the literature (Suppe and Medwedeff, 1990).

4. Conclusions

We have shown that the trishear zone need not be symmetric and that an unlimited number of velocity fields can be constructed based on incompressibility, continuity of the flow and matching of the basic boundary conditions of the model. All of these fields are 'trishear' by the original definition of Erslev (1991): "distributed, strain-compatible shear in a triangular (in profile) shear zone…". Such fields may or may not correspond to features seen in real structures; our purpose here is only to show that they can be derived and to provide a general method for doing so. The deformation resulting from any of these fields is easily computed by numerical integration. Although the strain rate singularity in the trishear model is consistent with results for a crack in an elastic–plastic material, it remains to be seen how consistent these models are with respect to mechanical models.

Acknowledgements

We thank Eric Erslev and Stuart Hardy for reviews of the manuscript. Allmendinger gratefully acknowledges support from the National Science Foundation (EAR-9814348).

References

Allmendinger, R.W., 1998. Inverse and forward numerical modeling of trishear fault-propagation folds. Tectonics 17, 640–656.

Erslev, E.A., 1991. Trishear fault-propagation folding. Geology 19, 617–620.

Erslev, E.A., Rogers, J.L., 1993. Basement–cover geometry of Laramide fault-propagation folds. In: Schmidt, C.J., Chase, R.B., Erslev, E.A. (Eds.), Laramide Basement Deformation in the Rocky Mountain Foreland of the Western United States, Geological Society of America Special Paper, 280, pp. 125–146.

Erslev, E.A., Mayborn, K.R., 1997. Multiple geometries and modes of fault-propagation folding in the Canadian thrust belt. Journal of Structural Geology 19, 321–335.

Hardy, S., Ford, M., 1997. Numerical modeling of trishear fault propagation folding. Tectonics 16, 841–854.

Hardy, S., McClay, K., 1999. Kinematic modeling of extensional fault-propagation folding. Journal of Structural Geology 21, 695–702.

Mase, G.E., Mase, G.T., 1992. Continuum Mechanics for Engineers. CRC Press, Boca Raton.

Rice, J.R., 1968. Mathematical analysis in the mechanics of fracture. In: Liebowitz, H. (Ed.), Fracture. An Advanced Treatise. Academic Press, New York, pp. 192–311.

Suppe, J., Medwedeff, D.A., 1990. Geometry and kinematics of fault-propagation folding. Eclogae Geologicae Helvetiae 83, 409–454.